Shock Waves
https://doi.org/10.1007/s00193-024-01158-5

ORIGINAL ARTICLE

Bilayer surrogate brain response under various blast loading conditions

C. Norris[1,2] · B. Arnold[1,2] · J. Wilkes[1,2] · C. Squibb[3] · A. J. Nelson[1,2] · H. Schwenker[2] · J. Mesisca[2] · A. Vossenberg[2] · P. J. VandeVord[1,2,4]

Received: 6 February 2023 / Revised: 2 January 2024 / Accepted: 3 January 2024

Abstract
Variations in the experimental constraints applied within blast simulations can result in dramatically different measured biomechanical responses. Ultimately, this limits the comparison of data between research groups and leads to further inquisitions about the "correct" biomechanics experienced in blast environments. A novel bilayer surrogate brain was exposed to blast waves generated from advanced blast simulators (ABSs) where detonation source, boundary conditions, and ABS geometry were varied. The surrogate was comprised of Sylgard 527 (1:1) as a gray matter simulant and Sylgard 527 (1:1.2) as a white matter simulant. The intracranial pressure response of this surrogate brain was measured in the frontal region under primary blast loading while suspended in a polyurethane spherical shell with 5 mm thickness and filled with water to represent the cerebrospinal fluid. Outcomes of this work discuss considerations for future experimental designs and aim to address sources of variability confounding interpretation of biomechanical responses.

Keywords Intracranial pressure · Blast exposure · Experimental design · Biofidelic · Brain surrogate · Material characterization

1 Introduction

Overpressures produced by explosive devices are known to cause primary blast-induced traumatic brain injury (bTBI). Primary bTBI results exclusively from the energy transfer from the blast overpressure to the brain tissue. To investigate the mechanics of primary bTBI, free-field explosions are replicated in a laboratory environment using blast simulators. It is crucial that these simulators replicate the blast physics idealized by the Friedlander waveform [1, 2]. In particular, the advanced blast simulator (ABS) was designed to generate overpressures with distinct positive and negative phases and contains an end-wave eliminator designed to prevent inadvertent shock and rarefaction waves from causing unwanted secondary insults to the test specimen [2]. ABS systems have been developed with variable cross-sectional areas of the test section ranging from 0.25 to 1.2 m [3–6] with both compressed gas and gas-detonation methods. However, experimental designs and imposed boundary conditions even within ABS systems are highly variable, which makes it difficult to compare experimental outcomes and ultimately determine which simulated responses are most representative of those experienced by military and civilian populations in regions of conflict. Therefore, the main purpose of this study was to show experimentally how changes in these design considerations may affect interpretation of brain mechanics under blast loading.

Brain mechanics are commonly measured by the changes in intracranial pressure (ICP) during a blast exposure as it provides a quantitative metric related to the stresses and strains imparted on the brain tissue. Previous studies have measured ICP during blast in preclinical models, such as rats [7–9] and pigs [10–12], which allows for comparison of the mechanics with the pathophysiological response to better understand bTBI. Postmortem human surrogate (PMHS)

Communicated by R. Banton, T. Piehler, R. Shoge.

✉ P. J. VandeVord
pvord@vt.edu

1 School of Biomedical Engineering and Sciences, Virginia Tech, Blacksburg, VA, USA

2 Department of Biomedical Engineering and Mechanics, Virginia Tech, Blacksburg, VA 24061, USA

3 Kevin T. Crofton Department of Aerospace and Ocean Engineering, Virginia Tech, Blacksburg, VA, USA

4 Veterans Affairs Medical Center, Salem, VA, USA

Published online: 05 April 2024

ICP has also been tested under blast loading [13, 14] aimed to define the human biomechanics. While the preclinical models are physiologically relevant and the PMHS is anatomically relevant, there are a number of limitations such as ethical considerations, restrictions on sample sizes, and subject-to-subject variability. To fill this gap, interest in the development of biofidelic surrogate models has been on the rise due to numerous advantages as a low-cost, repeatable alternative. Although the brain is comprised of two materials of varying stiffness, brain simulants are commonly tested as a uniform material such as gelatin [4, 15–20], biogel [21, 22], and silicone [16, 17, 19, 23–27]. These simulants containing a single material have been previously tested under blast loading [21, 23, 26, 28–30]. However, computational models show that high-level shear stresses between the cerebrospinal fluid (CSF) and brain tissue as well as the gray matter–white matter junctions influence the pressure distribution and overall understanding of bTBI mechanics [31–33]. Wermer et al. [20] recently introduced a highly complex bilayer surrogate model intended for blast testing that contained gray and white matter simulants from bovine and polyacrylamide gelatins and molded these materials into a surrogate skull with a central sulcus, simplified gyri, sulci, ventricles, and vasculature. Considering the influence that these structural complexities have on the biomechanical response during blast, we designed a novel bilayer brain surrogate composed of white and gray matter simulants and then utilized this new surrogate model to compare the ICP response during blast under various experimental conditions.

2 Experimental methods

2.1 Material characterization

Silicone gels were found to have more similar mechanical properties to brain tissue, leading to further investigation of polydimethylsiloxane (PDMS) simulants [15–18]. Sylgard 527 [15, 19, 24–27] and Sylgard 184 [23] (Dow Corning Corporation, Auburn, MI) have been tested as brain simulants upon varying the proportion of curing agent (part B) added to the base (part A). Chanda et al. [25] considered varying the proportions of part A and part B in a silicone gel material and tested the resulting mechanical properties relating to gray and white matter. Based on this reasoning, we decided to develop gray and white matter simulants by varying the A:B ratios of Sylgard 527. The gray matter simulant was mixed at a 1:1 ratio of the base (part A) to the curing agent (part B), while the white matter simulant was mixed at a ratio of 1:1.2. The elastic modulus of Sylgard 527 1:1 was previously reported to range from 1.04 to 5.0 kPa, consistent with the expected range for human gray matter [19, 34, 35]. However, the white matter elastic modulus is approximately 40% stiffer, and thus, the hardener ratio was increased [36]. The ratio of 1:1.2 was selected based on interpolation of the elastic modulus between tensile data collected at ratios of 1:1 and 1:2.

The isotropic elastic material properties were then determined for a set of performed uniaxial tension and compression tests. These tests were conducted according to ASTM D638 [37] and D575 [38] standards, respectively. Five samples were fabricated for each loading case and mixture ratio with Type I dogbone specimens for the tensile loading and cylindrical specimen geometries for compression testing. Examples of the negative molds are shown in Fig. 1a, b, and mean sample geometries are provided in Table 1. All samples were degassed for 10 min at 98.2 kPa (29″ Hg) in a vacuum chamber and cast in silicone and acrylic negative molds. Samples were then allowed to cure at 22 °C for 48 h before being removed prior to testing.

Mechanical testing was completed in a model 6800 Instron universal testing machine (Instron, Norwood, MA). Test profiles were displacement-controlled, with a crosshead displacement rate set to 10 mm/min, consistent with ASTM test standards, resulting in an effective strain rate of 1.6×10^{-3} s^{-1}. The end of test condition was achieved when an effective axial strain of 100% was reached in tension or 50% in compression. These test conditions were selected based on experimental constraints. Further, post-processing revealed instances of grip slipping and/or camera obstruction at deformations above 50% in tension and 20% in compression, and therefore, data beyond these limits were not analyzed. Surface strain measurements were taken through the gage sections of the samples using a two-camera digital image correlation (DIC) setup, as depicted in Fig. 1c, d, which was sampled at 0.5 Hz. Deformation fields were calculated using DaVis 10.2 software (LaVision Inc., Ypsilanti, MI) based on the two-camera DIC setup. Instron and DIC data were aligned in time, and the axial stress and effective axial and transverse strains were computed from the displacement fields (Fig. 1e, f). The two-camera DIC system was aligned with the loading direction of the Instron, which allowed for direct use of the axial and transverse displacement components from the DIC measurements. Young's modulus (E) was then estimated by fitting a linear regression line through the axial stress and strain data. The resulting elastic properties of the gray and white matter simulants were then compared to human tissue.

2.2 Bilayer surrogate brain

To develop the bilayer brain, a hemispheric mold was designed using CAD software (Autodesk, Mill Valley, CA) based on the assumption that gray matter thickness ranges

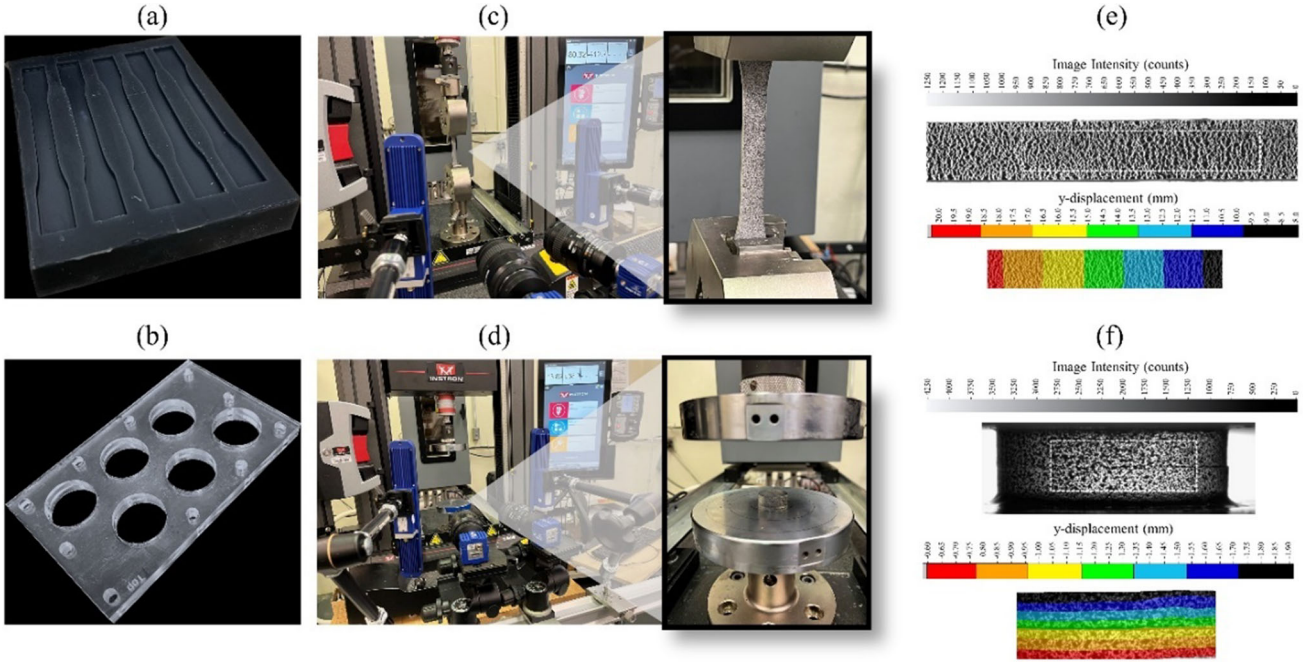

Fig. 1 Tension and compression fabrication and test setup. **a** Silicone negative mold for Type I dogbone tension samples and **b** acrylic negative mold for compression samples. **c** Test setup for tension samples and **d** compression samples, with speckled samples between crossheads and compression plates. **e** Processed axial displacement from tension and **f** compression test samples with view of speckled sample (top) and corresponding displacement fields (bottom)

Table 1 Geometries of tension and compression samples

Sylgard 527 (A:B)	Tension		Compression	
	Width (mm)	Thickness (mm)	Diameter (mm)	Thickness (mm)
1:1	12.50 ± 0.03	3.01 ± 0.04	28.56 ± 0.05	11.05 ± 0.12
1:1.2	12.49 ± 0.05	3.02 ± 0.05	28.55 ± 0.04	11.01 ± 0.07

Values reported as mean ± SD

from 1 to 4.5 mm [39]. To incorporate the two layers, inner white matter simulant volume (Sylgard 527 1:1.2) was reduced by 14% to allow for an approximately 4-mm-thick layer of gray matter simulant (Sylgard 527 1:1) along the outside of the mold. The brain dimensions were 116 mm left-right × 152 mm anterior−posterior × 79 mm superior–inferior with a volume of 789 cm^3. These dimensions are smaller than the average human brain (140 mm × 176 mm × 130 mm) [40], and improvements to this mold design may consider upscaling by at least 12% for future testing. However, this limitation was not expected to greatly influence the ICP comparisons between configurations. The stl files for the hemispheric molds can be downloaded in the Supplemental Information. Each file was 3D-printed on a Makerbot X (MakerBot Industries, LLC, Brooklyn, NY) with temperature-stable ABS plastic filament. Four support sticks were printed along with one inner piece and outer mold for the left hemisphere and one inner piece and outer mold for the right hemisphere. For each hemisphere, two support sticks were adhered to the flat side of the inner piece and rested on top of the outer mold (Fig. 2).

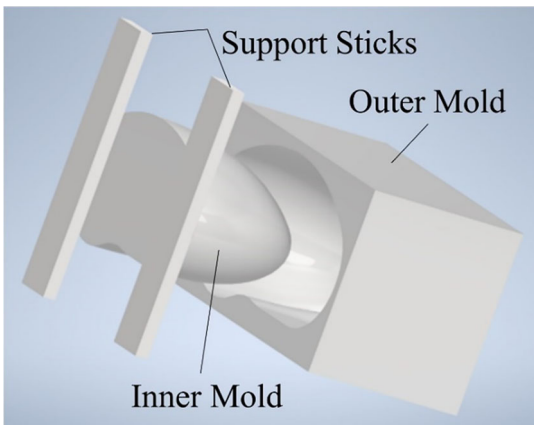

Fig. 2 Hemispheric bilayer mold configuration

The two hemispheric molds were then lined with polyvinyl alcohol (PVA) and plastic wrap to allow for easy material

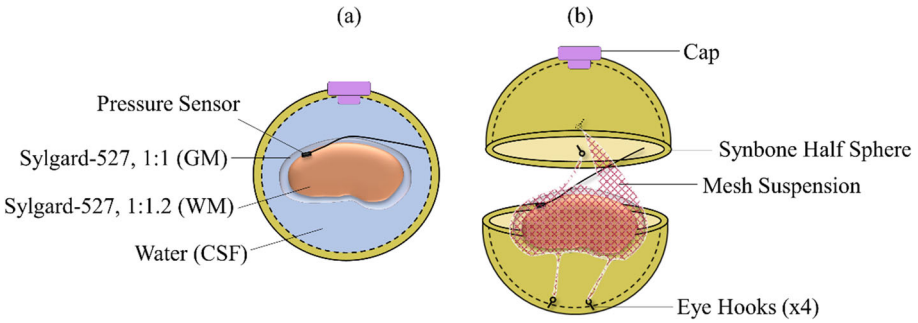

Fig. 3 Schematic of surrogate brain suspension within a SYNBONE® spherical shell. **a** Sagittal view of fluid-filled surrogate with pressure sensor placed in the frontal brain region where the gray matter (GM) simulant Sylgard 527 (1:1) and white matter simulant (WM) Sylgard 527 (1:1.2) layers met. **b** Expanded view of how the brain was suspended and attached to eye hooks within the surrogate sphere

separation once cured. The gray matter simulant of Sylgard 527 1:1 was then mixed, degassed, and slowly poured until it was level with the top edge. The molds were then placed in an oven at 100 °C for 3.5 h and allowed 15 min to cool once removed. The inner brain mold was then detached from the cured layer of Sylgard 527 1:1. The degassed Sylgard 527 1:1.2 white matter simulant was then poured until it was level with the top edge of the outer mold. After an additional 3.5 h at 100 °C, the hemispheres were removed from the oven, allowed to cool, extracted from their respective molds, and adhered to each other using Sil-Poxy (Smooth-On, Inc., Macungie, PA).

2.3 Instrumentation and suspension

To measure the ICP response under blast loading, the developed bilayer simulant needed to be instrumented and suspended within a surrogate skull. A Millar Mikro-tip Catheter Transducer (SPR-524; ADInstruments, Inc., Colorado Springs, CO) was placed in the frontal region of the brain surrogate between the boundary separating the gray and white matter simulants (Fig. 3a). ICP response in the frontal region is commonly measured and was selected in this study to allow for ease of comparison with other surrogate ICP responses to frontal blast loading. These pressure transducers have previously shown high performance under blast loading and are advantageous due to their small size (tip diameter equal to 1.2 mm) and sensitivity (1.296 mV/psi) [11, 41]. The brain was then suspended in a modified bone-like polyurethane spherical shell with 5 mm thickness and 190 mm diameter (SYNBONE®, Malans, Switzerland) by surrounding the brain in a mesh and attaching it to four eye hooks on the inside of the shell (Fig. 3b). The SYNBONE® half-spheres were bonded using an epoxy adhesive (J-B Weld Plastic Bonder), and the sphere was then filled with water to simulate the CSF. The opening at the top of the skull was sealed using a cap to ensure a closed system. These design selections were determined based on previous adoption of similar simplifications using spherical surrogates [4, 17, 18] and water as a CSF simulant [26, 27] under both impact and blast loading conditions. The use of a mesh suspension was a novel addition necessary to functionally suspend the brain and prevent large-scale movement or rotation. Although largely simplified, boundary conditions imparted by the mesh may be structurally relevant to the role of the meninges.

2.4 Blast configurations

Change in surrogate ICP under primary blast loading was measured for two different experimental configurations. Advanced blast simulators (ABSs) with varying gas and detonation type, test section area, and boundary conditions were considered (Table 2). ABS1 was a compressed helium-driven system that generated an overpressure from a membrane burst, which traveled down a 0.3 m × 0.3 m test section over the test specimen. ABS4 was a gas detonation system where the magnitude was governed by volumetric changes in oxygen and acetylene within the driver. The pressures within the ABS were measured on the walls of the 1.2 m × 1.2 m test section. In both cases, the ABS contained an end-wave eliminator to restrict reflections back on the test section as well as sensors along the test section wall to measure overpressure waveforms adjacent to the specimen (PCB Piezotronics, Inc., Depew, NY). In the ABS1 configuration, the surrogate was suspended in a taught mesh sling and in the ABS4 configuration, the surrogate was rigidly fixed to a metal post at the center of the test section (Fig. 4). For each configuration, duplicate ICP profiles were collected in response to static overpressure magnitudes of 117 kPa, which simulates mild bTBI conditions.

Data were acquired at 800 kHz using a TMX Multi-Channel High Speed Data Acquisition Recorder (AstroNova, Inc., West Warwick, RI). The resulting pressure traces were

Table 2 Comparison of testing configurations

	ABS1	ABS4
Gas	Helium	Oxygen + acetylene
Wave generation mechanism	Membrane burst	Gas detonation
Test section area	0.3 m × 0.3 m	1.2 m × 1.2 m
Boundary conditions	Hanging in a mesh sling	Bolted to a metal plate on the bottom surface

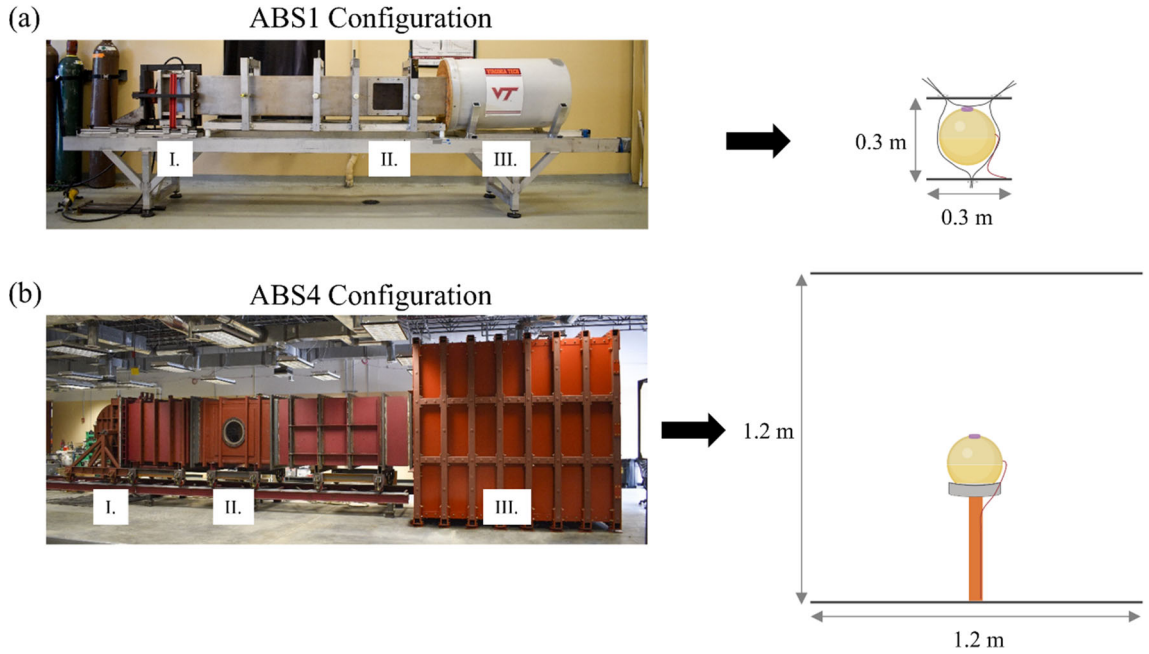

Fig. 4 ABS1 and ABS4 testing configurations. **a** The surrogate was placed in the ABS1 and secured in a taught mesh sling with three ring clasps. **b** The surrogate was placed in the ABS4 and secured to a metal plate with four screws. Each ABS consisted of a (I) driver, (II) test section, and (III) end-wave eliminator. As seen on the right, the specimen was located in the test section, and the surrounding dimensions are variable

exported, and all data were processed in MATLAB R2022a (MathWorks, Natick, MA). Offsets from baseline were corrected for all pressure traces. Filtering was not performed in order to preserve and examine frequency contributions. ICP characteristic curves as well as rise time, positive duration, peak pressure, and frequency response were compared in the ABS1 configuration versus the ABS4 configuration. Rise time was measured as the time from baseline to peak pressure at the arrival of the shock front and the positive duration was measured from the baseline just before the arrival of the shock front up until the pressure returned to zero. The ICP frequency response was measured manually as the inverse of the time between the first two oscillations (Supplemental Figure). Two-sided t-tests were performed to detect significant differences between ICP characteristics where $p < 0.05$ was significant.

3 Results and discussion

3.1 Brain simulant properties

To create biofidelic models, material properties should mimic the human brain tissue. The brain consists of two distinct types of cortical tissue: gray and white matter. Due to the low elastic modulus, nonlinear viscoelastic tissue response, and heterogeneity throughout the brain, a wide range of elastic moduli have been reported for both gray and white matter (Table 3). Material properties of ex vivo brain tissue have been measured under compression loading [23, 42, 43], indentation methods [36, 44, 45], and tensile loading [43]. An alternative method for measuring in vivo material properties using magnetic resonance elastography (MRE) has also been employed [46].

As shown in Table 3, the elastic modulus of brain tissue can be affected by loading condition, loading rate, brain region, in vivo versus ex vivo tissue conditions, and species. In this study, the elastic modulus was measured in tension and compression for a single loading rate of 1.6×10^{-3} s^{-1} consistent with ASTM standard testing. Engineering stress was plotted up to 50% axial strain under tensile loading (Fig. 5a) where the elastic modulus was 2.01 ± 0.15 kPa for Sylgard 527 (1:1) and 3.57 ± 0.14 kPa for Sylgard 527 (1:1.2). Engineering stress was plotted up to 20% axial strain under compressive loading (Fig. 5b) where the elastic modulus was 2.38 ± 0.48 kPa for Sylgard 527 (1:1) and 6.93 ± 0.73 kPa for Sylgard 527 (1:1.2). Downsampled data are provided in the Supplemental Information for reference. The modulus ranges were 2–4 kPa for the gray matter simulant (Sylgard 527 1:1) and 3.5–7 kPa for the white matter simulant (Sylgard 527 1:1.2), which fell within the anticipated range of human in vivo and ex vivo gray and white matter elastic moduli (Table 3).

Nevertheless, the viscoelastic and delicate nature of these soft materials render it difficult to validate the material response when tested under different loading rates and experimental setups. More specifically, the loading rate is known to have a significant effect on the elastic behavior of brain tissue such that an increased rate corresponds to an increased elastic modulus [23, 43, 47, 48]. There remains a significant need for standardization of methods for testing brain surrogates. Furthermore, although we showed that the Sylgard simulant formulations followed similar elastic properties to gray and white matter at low displacement rates, this work is not without limitations. Full characterization of the viscoelastic properties should be performed in future work to expand on these findings and assess the dynamic response at strain rates greater than 50 s^{-1} comparable to predicted conditions under blast loading [49–52].

Single material brain surrogates lack structural and material complexities that have been shown to influence blast-induced biomechanical responses predicted in computational models [31–33]. To best replicate biofidelic responses under blast loading, research efforts should aim to incorporate gray and white matter as well as structural complexities introduced by the ventricles and vasculature, similar to Wermer et al. [20]. Increased surrogate complexity was achieved in this study by combining two layers of Sylgard 527 in a brain mold to simulate gray and white matter. This detailed approach demonstrated feasibility and provided a means to compare the biomechanical responses under different experimental conditions. However, experimental testing comparing the ICP response with a single material versus added complexities should be performed in future iterations to validate the computational models.

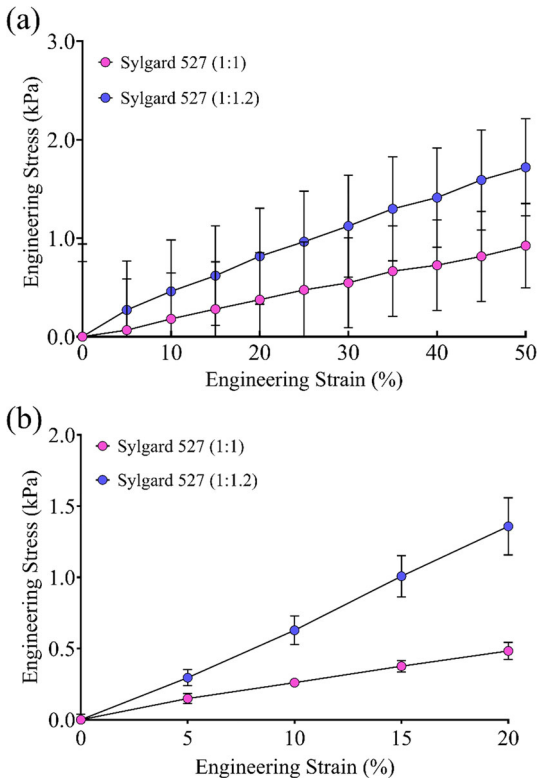

Fig. 5 Engineering stress (kPa) plotted against engineering strain (%) of Sylgard 527 (1:1) and (1:1.2) under **a** tension up to 50% strain and **b** compression up to 20% strain

3.2 Experimental design considerations

The instrumented surrogate was placed in two test configurations according to Table 2. Blast testing prior to the placement of the surrogate ensured calibration of the sensors within the ABS system and followed free-field blast conditions. Once the surrogate was secured in the ABS, the overpressure profiles surrounding the surrogate were analyzed to ensure free-field blast physics were replicated. The static overpressure 30 cm upstream of the test specimen in the ABS1 and 40 cm upstream in the ABS4 configurations (Fig. 6a) resulted in repeatability of the Friedlander waveforms with average peak overpressures of 118.1 ± 4.2 kPa. Visual comparison of these profiles upstream of the surrogate also demonstrates that the overpressure properties prior to contact with the surrogate remained consistent regardless of the mechanism of blast wave creation (membrane burst vs. gas detonation) or cross-sectional area (0.09 m^2 vs. 1.44 m^2). However, while the overpressures directly adjacent to the surrogate brain (Fig. 6b) were repeatable within each respective configuration, the ABS1 overpressures were amplified and contained significant fluctuations from the calibration profiles that were not representative of a clean Friedlander waveform, as indicated by the red arrows. These fluctuations are most likely wave reflections resulting from lack of clearance around the

Table 3 Human, porcine, and bovine elastic modulus (E) of gray and white matter calculated under different testing parameters compared to the current study

Study	Species	E (kPa)	Test parameters
White matter			
Jin et al. [43]	Human (ex vivo)	Compression: 10.96 ± 4.62 Tension: 3.13 ± 1.05	Tissue was loaded at 0.5 s^{-1} in compression and tension and values were calculated at 20% strain
Arjun et al. [44]	Human (ex vivo)	Motor cortex: 1.05 ± 0.14 Sensory cortex: 2.81 ± 0.16 Frontal cortex: 10.64 ± 1.93	Indentation
Huang et al. [46]	Human (in vivo)	3.36 ± 0.11 − 3.85 ± 0.12	MRE collected at 40–60 Hz
Kaster et al. [45]	Porcine	1.787 ± 0.186	Indentation
Budday et al. [36]	Bovine	1.895 ± 0.592	Indentation
Current study	Sylgard 527 (1:1.2)	Compression: 6.93 ± 0.73 Tension: 3.57 ± 0.14	Tissue was loaded at 1.6 × 10^{-3} s^{-1} in compression and tension and values were calculated at 20% and 50% strain, respectively
Gray matter			
Jin et al. [43]	Human (ex vivo)	Compression: 8.26 ± 7.22 Tension: 2.49 ± 0.90	Tissue was loaded at 0.5 s^{-1} in compression and tension and values were calculated at 20% strain
Arjun et al. [44]	Human (ex vivo)	Motor cortex: 0.33 ± 0.03 Sensory cortex: 1.18 ± 0.05 Frontal cortex: 1.29 ± 0.23	Indentation
Huang et al. [46]	Human (in vivo)	2.24 ± 0.14 − 3.33 ± 0.14	MRE collected at 40–60 Hz
Kaster et al. [45]	Porcine	1.195 ± 0.157	Indentation
Budday et al. [36]	Bovine	1.368 ± 0.289	Indentation
Current study	Sylgard 527 (1:1)	Compression: 2.38 ± 0.48 Tension: 2.01 ± 0.15	Tissue was loaded at 1.6 × 10^{-3} s^{-1} in compression and tension, and values were calculated at 20% and 50% strain, respectively
Whole brain			
Zhang et al. [23]	Porcine	2.618–11.176	Compression at a range of crosshead displacement rates up to 20% strain
Falland-Cheung et al. [42]	Porcine	2.44	Compression at a strain rate of 0.25 s^{-1} up to 20% strain

Values reported as mean ± SD

test specimen within the 0.3 m × 0.3 m area (Supplemental Figure). Although many blast configurations are limited by space, most agree that the test specimen should restrict less than 20% of the area or else the wave profiles become more complex and the flow streamline no longer simulates free-field blast conditions [53]. Blockage of the sphere in the ABS1 test section was 30% compared to 2% in the ABS4. Profiles shown in Fig. 6b demonstrate the influence of low clearance surrounding the test specimen on the overpressure blast physics. Upon further inspection, the reflections introduced by the surrogate in ABS1 are suspected to have influenced the corresponding ICP impulse (Fig. 6c) such that there is a large secondary peak in the ICP response, indicated by the red arrow. To avoid potential confounding effects within the biomechanical response, these data support recommendations to maintain ample clearance around the test specimen.

Surrogate biomechanical responses were found to be distinctly different in the ABS1 configuration compared to the ABS4 (Fig. 6c). When examining the ICP response, quantification and comparison of ICP profile characteristics can help distinguish whether the modes of energy transfer differ between configurations. The ICP profiles showed that the ABS1 configuration had a significantly greater rise time to peak pressure (0.148 ± 0.01 ms) and positive duration (0.90 ± 0.14 ms) compared to the ABS4 rise time (0.058 ± 0.00 ms) and positive duration (0.42 ± 0.00 ms). These major differences in biomechanical responses are most likely attributed to the variations in boundary conditions between configurations. More specifically, the imposed rigid constraint on the deformation of the spherical shell under frontal blast loading decreased the rise time and positive phase duration such that energy dissipation occurred at a higher rate compared to in the suspended mesh configuration.

This proposed influence of boundary conditions on the biomechanical response was further supported by comparing ICP traces from rigidly fixed surrogates to suspended,

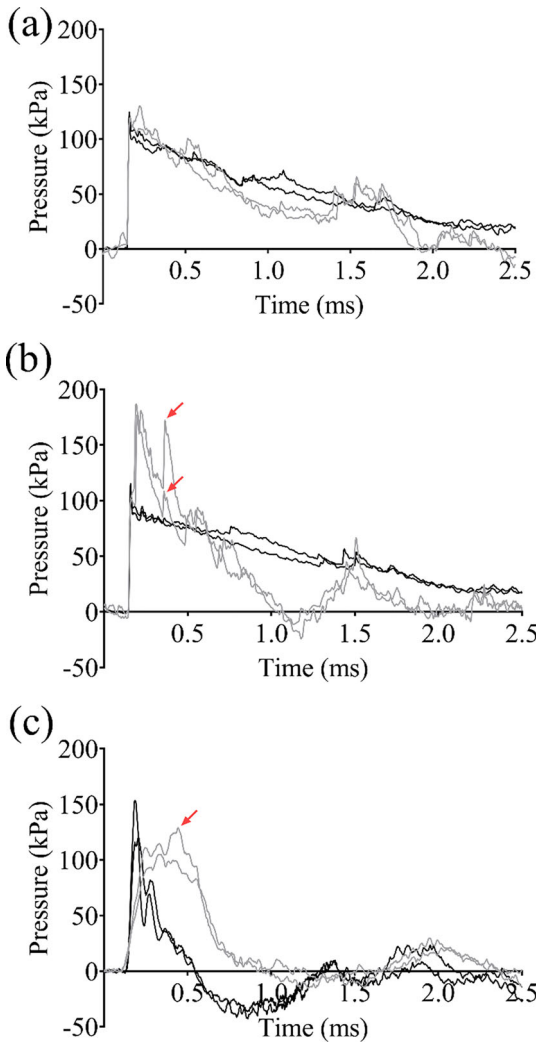

Fig. 6 Static overpressure and surrogate ICP comparison in the ABS1 (gray) and ABS4 (black). **a** Static overpressure upstream of the specimen, **b** static overpressure adjacent to the specimen, and **c** ICP response. Duplicate pulses are provided to demonstrate repeatability within each configuration. The red arrows indicate suspected contributions introduced by the test configuration

unconstrained PMHS responses. In Bir [14], ICP response of a PMHS was collected while suspended in a mesh and inverted inside of a cylindrical shock tube. The PMHS was located 125 cm from the end of a shock tube and exposed to 104 kPa. The resulting frontal ICP rise time and positive duration were approximately 0.2 and 0.8 ms, respectively. These results were reproduced in a surrogate head testing ICP response under the same boundary conditions in Ouellet et al. [54]. In contrast, studies by Goeller et al. [28], Banton et al. [21], and Du et al. [55] measured ICP of rigidly attached surrogate heads placed outside of a free-field blast simulator where the resulting frontal ICP rise time and positive duration were approximately 0.04 and 0.2 ms, respectively. It is possible that mounting of the specimen outside of the blast simulator, known as end-jet testing, may influence the free-field blast and subsequent ICP profiles [2, 53]. However, based on comparison of our data with previously reported data, we conclude that surrogate ICP profiles have longer rise times and positive phase durations when suspended in mesh compared to those rigidly mounted. This leads to the question of which boundary condition is more physiologically relevant.

The use of a semi-rigid neckform, such as a Hybrid III neck, has been previously employed to account for this boundary condition. Even though the flexural stiffness is greater than a human neck, it could provide less overall damping to the ICP response compared to a fully rigid support [30]. Ouellet et al. [30] and Azar et al. [26] used Sylgard 527 as a brain simulant and attached a head surrogate to a Hybrid III neck. Based on visual approximations, the frontal ICP rise time and positive durations fell between the rigid and suspended configuration boundaries. Further, it is possible that the "true" frontal ICP profile characteristics fall within this range. Future surrogate testing should consider a semirigid mounting configuration that accounts for similar neck properties at the base of the skull, as it was shown here that the mounting mode greatly influences the ICP dynamics.

Another consideration related to brain injury mechanics is the ICP frequency response. A distinct ICP frequency was visible over the first 0.2 ms in both ABS1 and ABS4 configurations (Fig. 6c) and ranged from 11 to 13 kHz. Evidence of these frequencies in other surrogates under frontal blast loading has been shown in Du et al. [55], Banton et al. [21], Ouellet et al. [30], and Goeller et al. [28]. Bir et al. [14, 56] and Leonardi et al. [57] also showed an initial frequency response in PMHS ICP under frontal blast loading. Low-frequency contributions on the order of 700 Hz in the PMHS and 1100–1200 Hz in the surrogate head are also commonly reported [54]. This low frequency was visible for both configurations around 1200 Hz in Fig. 6c. These frequencies have been linked to contributions from the surrounding skull flexure [7, 9, 55]. At high rates of skull deformation, the response of the coupled system between the skull, CSF, and brain tissue is sensitive to the constitutive material properties between interfaces [31, 32, 58, 59]. At the transition between gray and white matter, or the cortico-medullary junction, computational models have identified high shear stress and concentrated regions of increased ICP [31, 32]. ICP profile peak pressures and frequency responses were not found to be statistically significant between ABS1 and ABS4 configurations, which suggests that these metrics were less sensitive to differences in imposed boundary conditions compared to the rise time and positive phase duration and may be more sensitive to changes in constitutive material properties, as proposed by the computational models. Therefore, when the boundary

conditions imposed on the surrogate are not translational to human biofidelic constraints and the tested surrogate lacks structural and material complexities, the deformation fields across the surrogate skull and subsequent regional ICP profiles likely contain compounded errors.

4 Conclusions

A bilayer surrogate was exposed to frontal blast loading in two different configurations within ABS systems and the ICP response in the frontal region was compared. The following considerations summarize potential sources of variability confounding interpretation of biomechanical responses:

1. Baseline assessments of overpressure blast dynamics should be performed both pre- and post-surrogate placement within the test configuration. Surrogate obstruction of the ABS test section should not be greater than 20% as this led to overpressure amplifications and reflections that influenced the ICP response.
2. The imposed constraints on the surrogate (mesh suspension or fully rigid fixation) significantly influenced the ICP profile characteristics such as the rise time and positive duration. Surrogates with semi-rigid fixation resulted in ICP rise times and positive durations in-between mesh and fully rigid constraints. These findings suggest that both human and surrogate biomechanical responses are mostly driven by the boundary conditions that constrain the head during blast. Therefore, future studies should focus on ways to incorporate biofidelic neckform constraints on surrogate models in order to approach the "true" biomechanical response.
3. A bilayer surrogate brain was developed in this study using Sylgard 527 (1:1) as the gray matter simulant and Sylgard 527 (1:1.2) as the white matter simulant, which is a first step toward added complexity in surrogate models. Experimental surrogate models currently lack the complexity to validate computational findings, which motivates the need for future surrogates to include anatomically correct skin-skull-fluid-brain ratios.

Reducing these sources of variability in experimental blast testing of surrogates will ultimately improve the validation of computational models, streamline interpretation of results between research groups, and more accurately model brain mechanics under blast loading.

Supplementary Information The online version contains supplementary material available at https://doi.org/10.1007/s00193-024-01158-5.

Acknowledgements The authors would like to thank the Department of Biomedical Engineering and Mechanics for their support, especially Christopher Arena and Andy Muelenaer. Partial funding support was awarded by the Virginia Tech Institute for Critical Technology and Applied Science (ICTAS).

Declarations

Conflict of interest The authors disclose no competing financial or non-financial conflicts of interest.

References

1. Cernak, I.: Blast injuries and blast-induced neurotrauma: Overview of pathophysiology and experimental knowledge models and findings. In: Kobeissy, F.H. (ed.) Brain Neurotrauma: Molecular, Neuropsychological, and Rehabilitation Aspects, vol. 45. CRC Press/Taylor & Francis, Boca Raton (2015)
2. VandeVord, P.J., Leonardi, A.D., Ritzel, D.: Bridging the gap of standardized animals models for blast neurotrauma: methodology for appropriate experimental testing. Methods Mol. Biol. **1462**, 101–118 (2016). https://doi.org/10.1007/978-1-4939-3816-2_7
3. Arun, P., Wilder, D.M., Eken, O., Urioste, R., Batuure, A., Sajja, S., Van Albert, S., Wang, Y., Gist, I.D., Long, J.B.: Long-term effects of blast exposure: a functional study in rats using an advanced blast simulator. J. Neurotrauma **37**(4), 647–655 (2019). https://doi.org/10.1089/neu.2019.6591
4. Mediavilla Varas, J., Philippens, M., Meijer, S.R., van den Berg, A.C., Sibma, P.C., van Bree, J.L., de Vries, D.V.: Physics of IED blast shock tube simulations for mTBI research. Front. Neurol. **2**, 58 (2011). https://doi.org/10.3389/fneur.2011.00058
5. Vu, P.A., Tucker, L.B., Liu, J., McNamara, E.H., Tran, T., Fu, A.H., Kim, Y., McCabe, J.T.: Transient disruption of mouse home cage activities and assessment of orexin immunoreactivity following concussive- or blast-induced brain injury. Brain Res. **1700**, 138–151 (2018). https://doi.org/10.1016/j.brainres.2018.08.034
6. Rodriguez, U.A., Zeng, Y., Deyo, D., Parsley, M.A., Hawkins, B.E., Prough, D.S., DeWitt, D.S.: Effects of mild blast traumatic brain injury on cerebral vascular, histopathological, and behavioral outcomes in rats. J. Neurotrauma **35**(2), 375–392 (2018). https://doi.org/10.1089/neu.2017.5256
7. Bolander, R., Mathie, B., Bir, C., Ritzel, D., VandeVord, P.: Skull flexure as a contributing factor in the mechanism of injury in the rat when exposed to a shock wave. Ann. Biomed. Eng. **39**(10), 2550–2559 (2011). https://doi.org/10.1007/s10439-011-0343-0
8. Chavko, M., Koller, W.A., Prusaczyk, W.K., McCarron, R.M.: Measurement of blast wave by a miniature fiber optic pressure transducer in the rat brain. J. Neurosci. Methods **159**(2), 277–281 (2007). https://doi.org/10.1016/j.jneumeth.2006.07.018
9. Dal Cengio Leonardi, A., Keane, N.J., Hay, K., Ryan, A.G., Bir, C.A., VandeVord, P.J.: Methodology and evaluation of intracranial

pressure response in rats exposed to complex shock waves. Ann. Biomed. Eng. **41**(12), 2488–2500 (2013). https://doi.org/10.1007/s10439-013-0850-2
10. Feng, K., Zhang, L., Jin, X., Chen, C., Kallakuri, S., Saif, T., Cavanaugh, J., King, A.: Biomechanical responses of the brain in swine subject to free-field blasts. Front. Neurol. **7**, 1–12 (2016). https://doi.org/10.3389/fneur.2016.00179
11. Shridharani, J., Wood, G., Panzer, M., Capehart, B., Nyein, M., Radovitzky, R., Bass, C.: Porcine head response to blast. Front. Neurol. **3**, 1–12 (2012). https://doi.org/10.3389/fneur.2012.00070
12. Sundaramurthy, A., Kote, V.B., Pearson, N., Boiczyk, G.M., McNeil, E.M., Nelson, A.J., Subramaniam, D.R., Rubio, J.E., Monson, K., Hardy, W.N., VandeVord, P.J., Unnikrishnan, G., Reifman, J.: A 3-D finite-element minipig model to assess brain biomechanical responses to blast exposure. Front. Bioeng. Biotechnol. **9**, 757755 (2021). https://doi.org/10.3389/fbioe.2021.757755
13. Iwaskiw, A.S., Ott, K.A., Armiger, R.S., Wickwire, A.C., Alphonse, V.D., Voo, L.M., Carneal, C.M., Merkle, A.C.: The measurement of intracranial pressure and brain displacement due to short-duration dynamic overpressure loading. Shock Waves **28**, 63–83 (2018). https://doi.org/10.1007/s00193-017-0759-z
14. Bir, C.: Measuring Blast-related Intracranial Pressure within the Human Head. Technical Report ADA547306, Wayne State University, Detroit, MI (2011)
15. Zhang, J., Yoganandan, N., Pintar, F.A., Guan, Y., Gennarelli, T.A.: Experimental model for civilian ballistic brain injury biomechanics quantification. J. Biomech. **40**(10), 2341–2346 (2007). https://doi.org/10.1016/j.jbiomech.2006.10.021
16. Hossain, S.: Material Modeling and Analysis for the Development of a Realistic Blast Headform. M.S. Thesis, University of Nebraska at Lincoln, Lincoln, NE (2010)
17. Alley, M.D., Schimizze, B.R., Son, S.F.: Experimental modeling of explosive blast-related traumatic brain injuries. Neuroimage **54**, S45–S54 (2011). https://doi.org/10.1016/j.neuroimage.2010.05.030
18. Singh, A., Ganpule, S.G., Khan, M.K., Iqbal, M.A.: Measurement of brain simulant strains in head surrogate under impact loading. Biomech. Model. Mechanobiol. **20**(6), 2319–2334 (2021). https://doi.org/10.1007/s10237-021-01509-6
19. Singh, D., Boakye-Yiadom, S., Cronin, D.S.: Comparison of porcine brain mechanical properties to potential tissue simulant materials in quasi-static and sinusoidal compression. J. Biomech. **92**, 84–91 (2019). https://doi.org/10.1016/j.jbiomech.2019.05.033
20. Wermer, A., Kerwin, J., Welsh, K., Mejia-Alvarez, R., Tartis, M., Willis, A.: Materials characterization of cranial simulants for blast-induced traumatic brain injury. Mil. Med. **185**(Supplement_1), 205–213 (2020). https://doi.org/10.1093/milmed/usz228
21. Banton, R., Piehler, T., Zander, N., Benjamin, R., Mrozek, R., Duckworth, J., Petel, O.: Experimental and numerical investigation of blast wave impact on a surrogate head model. Shock Waves **31**(5), 481–498 (2021). https://doi.org/10.1007/s00193-021-01033-7
22. Mrozek, R.A., Leighliter, B., Gold, C.S., Beringer, I.R., Yu, J.H., VanLandingham, M.R., Moy, P., Foster, M.H., Lenhart, J.L.: The relationship between mechanical properties and ballistic penetration depth in a viscoelastic gel. J. Mech. Behav. Biomed. Mater. **44**, 109–120 (2015). https://doi.org/10.1016/j.jmbbm.2015.01.001
23. Zhang, L., Jackson, W.J., Bentil, S.A.: The mechanical behavior of brain surrogates manufactured from silicone elastomers. J. Mech. Behav. Biomed. Mater. **95**, 180–190 (2019). https://doi.org/10.1016/j.jmbbm.2019.04.005
24. Zhu, F., Wagner, C., Dal Cengio Leonardi, A., Jin, X., VandeVord, P., Chou, C., Yang, K.H., King, A.I.: Using a gel/plastic surrogate to study the biomechanical response of the head under air shock loading: a combined experimental and numerical investigation. Biomech. Model. Mechanobiol. **11**(3), 341–353 (2012). https://doi.org/10.1007/s10237-011-0314-2
25. Chanda, A., Callaway, C., Clifton, C., Unnikrishnan, V.: Biofidelic human brain tissue surrogates. Mech. Adv. Mater. Struct. **25**(15–16), 1335–1341 (2018). https://doi.org/10.1080/15376494.2016.1143749
26. Azar, A., Bhagavathula, K.B., Hogan, J., Ouellet, S., Satapathy, S., Dennison, C.R.: Protective headgear attenuates forces on the inner table and pressure in the brain parenchyma during blast and impact: An experimental study using a simulant-based surrogate model of the human head. J. Biomech. Eng. **142**(4), 041009 (2019). https://doi.org/10.1115/1.4044926
27. Li, Y., Ouellet, S., Vette, A.H., Raboud, D., Martin, A., Dennison, C.R.: Evaluation of the kinematic biofidelity and inter-test repeatability of global accelerations and brain parenchyma pressure for a head-brain physical model. J. Biomech. Eng. **143**(9), 091006 (2021). https://doi.org/10.1115/1.4050752
28. Goeller, J., Wardlaw, A., Treichler, D., O'Bruba, J., Weiss, G.: Investigation of cavitation as a possible damage mechanism in blast-induced traumatic brain injury. J. Neurotrauma **29**(10), 1970–1981 (2012). https://doi.org/10.1089/neu.2011.2224
29. Hua, Y., Kumar Akula, P., Gu, L., Berg, J., Nelson, C.A.: Experimental and numerical investigation of the mechanism of blast wave transmission through a surrogate head. J. Comput. Nonlinear Dyn. **9**(3), 031010 (2014). https://doi.org/10.1115/1.4026156
30. Ouellet, S., Philippens, M.: The multi-modal responses of a physical head model subjected to various blast exposure conditions. Shock Waves **28**(1), 19–36 (2018). https://doi.org/10.1007/s00193-017-0771-3
31. Wang, C., Pahk, J.B., Balaban, C.D., Miller, M.C., Wood, A.R., Vipperman, J.S.: Computational study of human head response to primary blast waves of five levels from three directions. PLoS ONE **9**(11), e113264 (2014). https://doi.org/10.1371/journal.pone.0113264
32. Taylor, P.A., Ford, C.C.: Simulation of blast-induced early-time intracranial wave physics leading to traumatic brain injury. J. Biomech. Eng. **131**(6), 061007 (2009). https://doi.org/10.1115/1.3118765
33. Cernak, I.: Understanding blast-induced neurotrauma: how far have we come? Concussion **2**(3), CNC42 (2017). https://doi.org/10.2217/cnc-2017-0006
34. Moraes, C., Labuz, J.M., Shao, Y., Fu, J., Takayama, S.: Supersoft lithography: Candy-based fabrication of soft silicone microstructures. Lab Chip **15**(18), 3760–3765 (2015). https://doi.org/10.1039/c5lc00722d
35. Bouattour, Y., Sautou, V., Hmede, R., El Ouadhi, Y., Gouot, D., Chennell, P., Lapusta, Y., Chapelle, F., Lemaire, J.J.: A minireview on brain models simulating geometrical, physical, and biochemical properties of the human brain. Front. Bioeng. Biotechnol. **10**, 818201 (2022). https://doi.org/10.3389/fbioe.2022.818201
36. Budday, S., Nay, R., de Rooij, R., Steinmann, P., Wyrobek, T., Ovaert, T.C., Kuhl, E.: Mechanical properties of gray and white matter brain tissue by indentation. J. Mech. Behav. Biomed. Mater. **46**, 318–330 (2015). https://doi.org/10.1016/j.jmbbm.2015.02.024
37. ASTM D638-22: Standard Test Method for Tensile Properties of Plastics. ASTM International, West Conshohocken (2022). https://doi.org/10.1520/D0638-22
38. ASTM D575-91: Standard Test Methods for Rubber Properties in Compression. ASTM International, West Conshohocken (2018). https://doi.org/10.1520/D0575-91R18
39. Fischl, B., Dale, A.M.: Measuring the thickness of the human cerebral cortex from magnetic resonance images. Proc. Natl. Acad. Sci. USA **97**(20), 11050–11055 (2000). https://doi.org/10.1073/pnas.200033797
40. Lancaster, J.L., Tordesillas-Gutiérrez, D., Martinez, M., Salinas, F., Evans, A., Zilles, K., Mazziotta, J.C., Fox, P.T.: Bias between

MNI and Talairach coordinates analyzed using the ICBM-152 brain template. Hum. Brain Mapp. **28**(11), 1194–1205 (2007). https://doi.org/10.1002/hbm.20345
41. Bustamante, M.C., Singh, D., Cronin, D.S.: Polymeric Hopkinson bar-confinement chamber apparatus to evaluate fluid cavitation. Exp. Mech. **58**(1), 55–74 (2018). https://doi.org/10.1007/s11340-017-0323-x
42. Falland-Cheung, L., Scholze, M., Hammer, N., Waddell, J.N., Tong, D.C., Brunton, P.A.: Elastic behavior of brain simulants in comparison to porcine brain at different loading velocities. J. Mech. Behav. Biomed. Mater. **77**, 609–615 (2018). https://doi.org/10.1016/j.jmbbm.2017.10.026
43. Jin, X., Zhu, F., Mao, H., Shen, M., Yang, K.H.: A comprehensive experimental study on material properties of human brain tissue. J. Biomech. **46**(16), 2795–2801 (2013). https://doi.org/10.1016/j.jbiomech.2013.09.001
44. Arjun, B., Sitaramgupta, V.S.N.V., Aswin, S., Rao, S., Pandya, H.J.: A system-based approach for the evaluation of electromechanical properties of brain tumors. 44th Annual International Conference of the IEEE Engineering in Medicine & Biology Society (EMBC) (2022). https://doi.org/10.1109/EMBC48229.2022.9871879
45. Kaster, T., Sack, I., Samani, A.: Measurement of the hyperelastic properties of ex vivo brain tissue slices. J. Biomech. **44**(6), 1158–1163 (2011). https://doi.org/10.1016/j.jbiomech.2011.01.019
46. Huang, X., Chafi, H., Matthews, K.L., Carmichael, O., Li, T., Miao, Q., Wang, S., Jia, G.: Magnetic resonance elastography of the brain: a study of feasibility and reproducibility using an ergonomic pillow-like passive driver. Magn. Reson. Imaging **59**, 68–76 (2019). https://doi.org/10.1016/j.mri.2019.03.009
47. Miller, K., Chinzei, K.: Mechanical properties of brain tissue in tension. J. Biomech. **35**(4), 483–490 (2002). https://doi.org/10.1016/S0021-9290(01)00234-2
48. Rashid, B., Destrade, M., Gilchrist, M.D.: Mechanical characterization of brain tissue in tension at dynamic strain rates. J. Mech. Behav. Biomed. Mater. **33**, 43–54 (2014). https://doi.org/10.1016/j.jmbbm.2012.07.015
49. Hosseini-Farid, M., Amiri-Tehrani-Zadeh, M., Ramzanpour, M., Ziejewski, M., Karami, G.: The strain rates in the brain, brainstem, dura, and skull under dynamic loadings. Math. Comput. Appl. **25**(2), 21 (2020). https://doi.org/10.3390/mca25020021
50. Laksari, K., Assari, S., Seibold, B., Sadeghipour, K., Darvish, K.: Computational simulation of the mechanical response of brain tissue under blast loading. Biomech. Model. Mechanobiol. **14**(3), 459–472 (2015). https://doi.org/10.1007/s10237-014-0616-2
51. Zhang, J., Song, B., Pintar, F.A., Yoganandan, N., Chen, W., Gennarelli, T.A.: How to test brain and brain simulant at ballistic and blast strain rates. Biomed. Sci. Instrum. **44**, 129–134 (2008)
52. Ganpule, S.G., Alai, A.L., Plougonven, E., Chandra, N.: Mechanics of blast loading on the head models in the study of traumatic brain injury using experimental and computational approaches. Biomech. Model. Mechanobiol. **12**, 511–531 (2013). https://doi.org/10.1007/s10237-012-0421-8
53. Needham, C.E., Ritzel, D., Rule, G.T., Wiri, S., Young, L.: Blast testing issues and TBI: experimental models that lead to wrong conclusions. Front. Neurol. **6**, 72 (2015). https://doi.org/10.3389/fneur.2015.00072
54. Ouellet, S., Bir, C., Bouamoul, A.: Direct Comparison of the Primary Blast Response of a Physical Head Model with Post-Mortem Human Subjects. Technical Report DRDC-RDDC-2014-P113, Defence Research and Development Canada-Valcartier Research Center Quebec, QC Canada (2014)
55. Du, Z., Li, Z., Wang, P., Wang, X., Zhang, J., Zhuang, Z., Liu, Z.: Revealing the effect of skull deformation on intracranial pressure variation during the direct interaction between blast wave and surrogate head. Ann. Biomed. Eng. **50**(9), 1038–1052 (2022). https://doi.org/10.1007/s10439-022-02982-5
56. Bir, C., Bolander, R., Leonardi, A.D., Ritzel, D., VandeVord, P., Dingell, J.D.: A Biomechanical Prospective of Blast Injury Neurotrauma. A Survey of Blast Injury Across the Full Landscape of Military Science. Technical Report RTO-MP-HFM-207, North Atlantic Treaty Organization Science and Technology Organization (2011)
57. Leonardi, A.D.C.: An Investigation of the Biomechanical Response from Shock Wave Loading to the Head. PhD Thesis, Wayne State University, Detroit, MI (2011)
58. Chen, Y., O'Shaughnessy, T.J., Kamimori, G.H., Horner, D.M., Egnoto, M.J., Bagchi, A.: Role of interfacial conditions on blast overpressure propagation into the brain. Front. Neurol. **11**, 1–10 (2020). https://doi.org/10.3389/fneur.2020.00323
59. Gu, L., Chafi, M.S., Ganpule, S., Chandra, N.: The influence of heterogeneous meninges on the brain mechanics under primary blast loading. Compos. B Eng. **43**(8), 3160–3166 (2012). https://doi.org/10.1016/j.compositesb.2012.04.014